MIT Open Access Articles

Design Principles for Energy-Efficient Legged Locomotion and Implementation on the MIT Cheetah Robot

Massachusetts Institute of Technology

Design Principles for Energy Efficient Legged Locomotion and Implementation on the MIT Cheetah Robot

Sangok Seok[1], Albert Wang[1], Meng Yee (Michael) Chuah[1], Dong Jin Hyun[1], Jongwoo Lee[1], David Otten[2], Jeffrey Lang[2], and Sangbae Kim[1]

Abstract—This paper presents the design principles for highly efficient legged robots, the implementation of the principles in the design of the MIT Cheetah, and the analysis of the high-speed trotting experimental results. The design principles were derived by analyzing three major energy-loss mechanisms in locomotion: heat losses from the actuators, friction losses in transmission, and the interaction losses caused by the interface between the system and the environment. Four design principles that minimize these losses are discussed: employment of high torque density motors, energy regenerative electronic system, low loss transmission, and a low leg inertia. These principles were implemented in the design of the MIT Cheetah; the major design features are large gap diameter motors, regenerative electric motor drivers, single-stage low gear transmission, dual coaxial motors with composite legs, and the differential actuated spine. The experimental results of fast trotting are presented; the 33kg robot runs at 22 km/h (6 m/s). The total power consumption from the battery pack was 973 watts and resulted in a total cost of transport of 0.5, which rivals running animals' at the same scale. The 76% of total energy consumption is attributed to heat loss from the motor, and the 24% is used in mechanical work, which is dissipated as interaction loss as well as friction losses at the joint and transmission.

Index Terms—efficiency, legged locomotion, cost of transport, energy regeneration, quadrupeds robot
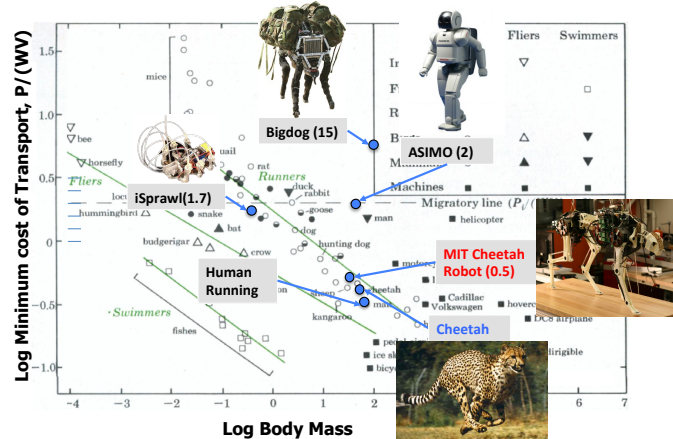

Fig. 1: Plot of total cost of transport (TCoT) vs body weight of animals and selected robots. The three classes of animal locomotion (running, flying, and swimming), occupy distinct regions of the plot. Used with permission from author of [2].

I. INTRODUCTION

ENERGY efficiency is a critical attribute that enables the successful use of legged robots in real applications. The ability to travel a long distance without recharging is crucial in tasks such as search-and-rescue and disaster response missions.

Although recent technological advances in legged robots have led to the ability to walk or run on flat and rough terrains, the energy efficiency of these robots is still notably worse than biological walkers or runners of a similar scale. The most widely used criterion for energy efficiency of legged locomotion is total cost of transport(TCoT: =P/WV), which is the ratio of power consumption to weight times velocity[1].

The TCoT of these robots is plotted on Tucker's animal data [2] in Fig. 1. As is shown by two of the most successful robots, the TCoT of ASIMO and Boston Dynamics BigDog are significantly higher than those of humans or animals of

[1]Authors are with the Department of Mechanical Engineering, Massachusetts Institute of Technology, Cambridge, MA, 02139, USA , corresponding email: `sangok at mit.edu`, Phone: `617-715-4309`

[2]Authors are with the Department of Electrical Engineering and Computer Science, Massachusetts Institute of Technology, Cambridge, MA, 02139, USA

The preliminary version of this paper has been presented [13]. This paper includes additional experimental results.

similar mass scale [2], [3]. Considering that the conversion efficiency in engineering actuators (e.g., from electricity to mechanical work) can be more efficient than the counterpart of biological system (from fat to mechanical work, ranging 20-25% [4]), there should be considerable room for improvement in current legged robots.

To date there have been two main approaches to improve the efficiency of legged robots: passive dynamics and elastic elements. Since legged locomotion involves highly unsteady usage of actuator power and alternating positive and negative work, these approaches provide 'mechanical energy capacitors' that can store kinetic or elastic potential energy and return without consuming significant energy.

The concept of passive dynamic walking was successfully implemented in walking robots and experimentally proven to improve energy efficiency. The Cornell Ranger exploited the passive dynamics of swing legs [1], [5]: its lowest recorded TCoT is 0.19. This locomotion efficiency is far superior to that of animals of the same scale. However, this robot sacrifices versatility in order to maximize its employment of the passive dynamics of human walking, and so its locomotion is restricted to a particular speed in fairly flat terrain, whereas ASIMO and BigDog are highly versatile [1].

Several robots employ series elastic actuators to utilize the energy recovery of mechanical springs [6], [7] and successfully demonstrated stable locomotion. One of the most efficient robots using this method successfully is iSprawl [8].

System Energy Flow
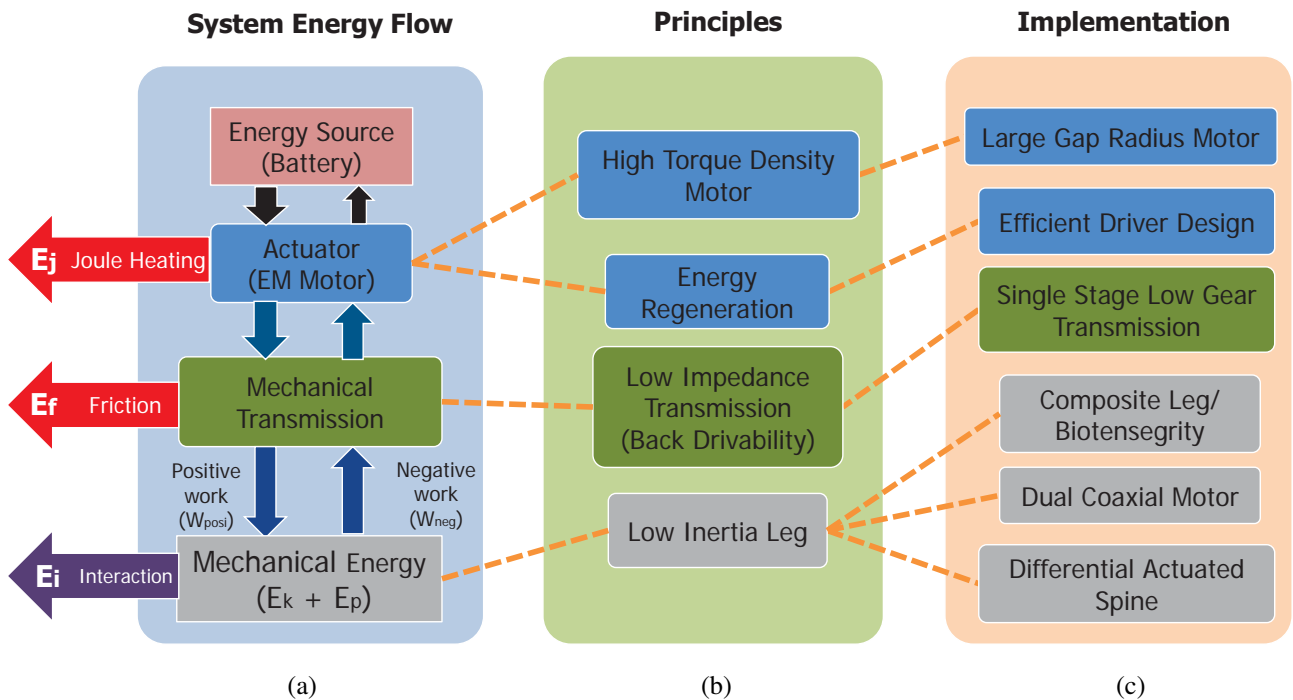
Principles

Implementation

Fig. 2: (a) Energy flow diagram of the robot showing energy flows between the source and mechanical energy. Joule heating loss occurs at the motor, friction loss occurs in the mechanical transmission and interaction loss reduces the total mechanical energy. (b) Design principles to improve efficiency at the sources of energy loss. (c) Strategies for implementing the design principles for efficiency used on the MIT Cheetah Robot.

It achieved a TCoT of 1.7, which matches animals efficiency as shown in Fig.1. However, this robot sets the stiffness of the series elastic spring as 14Hz of stride frequency, so it becomes less stable in lower frequency running. Hence, altering stiffness for stable locomotion over a wide range of speeds or ground stiffness becomes a challenge. One way to solve these problems is to use additional small actuators [9] dedicated for stiffness adjustments, but this can result in increased system complexity, extra weight, and additional energy consumption.

Another approach that utilizes elastic energy storage is employing parallel mechanical springs [10]. Instead of adding mechanical springs in series, this approach suggests finding an optimum stiffness and no-load position for springs in parallel to joint actuators. The idea was implemented in a dynamic simulation of a bounding quadruped model, and the results show that employing parallel springs can reduce the total power consumption by 15%, and, if switchable springs are implemented, by 53%.

Because the energy exchange through these mechanical elements is governed by passive dynamics, these approaches tend to be tuned for only a narrow range of speeds. Furthermore, these approaches are intended to minimize mechanical work and often do not directly address the energy loss associated with actuator itself.

In order to develop energy-efficient robots, we need to understand the energy loss mechanisms associated with the entire system. Energy efficiency is one of the most frequently used cost functions in optimizing control parameters in legged

robots. However, most optimization processes in the literature use only the mechanical cost of transport as a cost function, which is independent from energy dissipation such as joule heating of coils in electromagnetic actuators and transmission loss. Such approach provide a incomplete solution for optimum efficiency, considering that mechanical cost of transport contributes only a fraction of the total cost of transport, as shown in several robots (Cornell Ranger: MCoT/TCoT=0.21 [11], ATRIAS: MCoT/TCoT=0.24∼0.4 [12], MIT Cheetah: MCoT/TCoT=0.26 [13]). Furthermore, there have been few discussions on minimizing energy loss caused by actuators and few design methodologies or comprehensive design principles to maximize locomotion efficiency. It has been noted that the characteristics of actuation systems not only govern dynamic behavior but also characterize the energy flow in the robot. Therefore, there are opportunities to improve efficiency by optimizing actuator and mechanism design as a whole system.

It is remarkable that the term 'efficiency' in locomotion represented by TCoT is inherently different from the generic concept of efficiency used in a machine: the ratio of input power to output power. The locomotive system does not have an output as conventional machines if they travel on relatively flat ground, because the net change of the mechanical energy of the system is zero. The entire amount of energy reduced at the energy source is dissipated through locomotion. Therefore, locomotion in general is an energy dissipative process, and losses occur throughout the energy flow path from energy source to interactions with the environment. This is why the denominator of TCoT is a product of the magnitudes of two

orthogonal vectors (mass times gravity times horizontal speed) instead of a dot-product of two vectors, which would yield zero [1].

Considering that legged locomotion is an inherently dissipative process, simply increasing the energy efficiency of the actuator does not necessarily become a solution for more efficient locomotion. For example, machine designers often choose the actuator and gear ratios based on the torque requirement and the maximum efficiency speed. There are several drawbacks to this conventional approach. First, the speed-torque curve of locomotion of the actuator is highly dependent on three interdependent variables: 1) the dynamics of the running gait, 2) the dynamics of the transmission and actuator and 3) the control algorithms. In particular, the transmission ratio plays a crucial role in the overall leg impedance and control bandwidth. Second, since the net mechanical energy change is zero, the kinetic energy that is not dissipated by interaction loss or transmission loss should be recycled. This means the energy efficiency analyses should be done at every energy flow shown in Fig. 2 to calculate overall energy efficiency.

In order to provide design insights for developing energy-efficient robots, this paper introduces design principles for achieving high energy efficiency by analyzing energy loss throughout the entire system: actuator loss, transmission loss, and interaction loss. The next section explains these three energy loss mechanisms in legged locomotion and proposes design principles that can minimize the losses. Section III introduces how the design principles are implemented in the MIT Cheetah robot. Section IV demonstrates various experimental results and shows the system performance by comparing the cost of transport of the MIT Cheetah robot with animals and other robots. Finally, Section V discusses the conclusions and future work.

II. DESIGN PRINCIPLES FOR EFFICIENCY

In arriving at practical design principles for energy efficiency in legged robots, understanding energy flow is a critical step. It is important to analyze every possible pathway by which energy flows within a robot during locomotion. In Fig. 2, the leftmost column represents the energy flow of the robot. The three main energy-loss mechanisms in the flow are described below. The first loss is heat loss at the force transducer. In an electromagnetic (EM) motor, this is largely comprised of Joule heating, $E_j = I^2 R$; a minor component is the parasitic amplifier switching loss. The second is transmission loss, E_f. In a typical robot, this includes all losses through force transmission paths, such as friction losses at gears, belts, and bearings. The third energy-loss mechanism is interaction loss, including all the losses caused at the system boundary, which is the interface between the robot and the environment. Major sources of this loss in legged locomotion are foot impacts and air drag. The design of the robot needs to consider all of these factors to minimize overall loss.
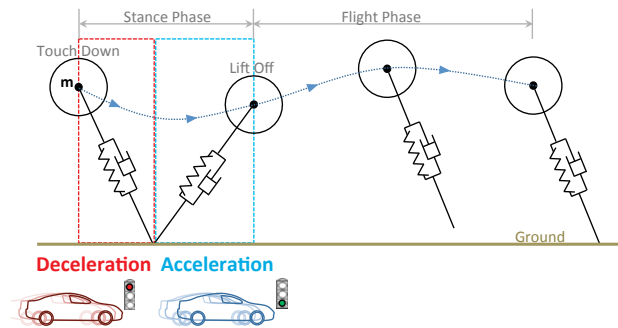

Fig. 3: Energy Regeneration as it occurs in a SLIP model. During landing, there is deceleration which charges the battery, and during jumping, the battery supplies the energy for acceleration.

We propose four design principles essential to the design of efficient legged robots. These principles shown in Fig. 2(b) directly address the three losses as denoted by the dotted lines.

A. Principle 1:High Torque Density Motor

This design principle suggests employing high-torque density EM motors for minimizing energy loss in actuators. This principle directly concerns the Joule heating of the EM motor by reducing the required electric current to provide torque for the locomotion. Here, the term torque density refers mass-specific continuous torque. If we assume the heat dissipation characteristic[2] of the motor remains same, the continuous torque of the motor represents how much torque the motor can generate at a constant heat dissipation. If we ignore the variations of the heat dissipation characteristics, the continuous torque is directly related to motor constant ($K_M = \tau / \sqrt{I^2 R}$), which represents torque per Joule heating. For example, if the torque density of the motor doubles without changing other factors such as the mass of the motor and heat dissipation characteristics, the Joule heating E_j can be reduced by 75%. In general, if the design parameters of the motor is optimized for the torque density, the coil mass increases and the stator steel mass decreases, which results in low peak torque. The motor should be designed also considering the maximum torque of the locomotion within the peak torque, where the torque-electric current relationship starts becoming non-linear due to magnetic flux saturation. At a given torque requirement, therefore, increasing the torque density of the EM motor is highly desirable for efficient locomotion without compromising the dynamics of the system.

B. Principle 2:Energy Regeneration

As discussed above, legged locomotion involves dynamic bidirectional energy flow from the energy source to the interaction with the ground. In legged locomotion, even in steady-state running, there are periods in each stride in which the leg

---

[1]For the same reason, we use miles-per-gallon to represent the fuel economy of a car, instead of efficiency as a percentage.

[2]The continuous heat dissipation power capability of the motor is dependent on the thermal resistance and the temperature difference between of the motor and environment; we assume this value does not change if the motor mass is similar.

does negative work [14]. These periods include the beginning of the ground phases and the ending of the swing phase where the torques and angular velocities are in the opposite direction to each other. Similar to the regenerative braking in electric cars, it is desirable to recover that energy rather than dissipating it in dampers and brakes [15].

Such energy recovery can be done by employing Series Elastic Actuation (SEA). An elastic element is placed between the actuator and the end effector that can temporarily store and release energy from ground contact. If the stiffness of the spring is well tuned for the natural dynamics of the body given by the running speed, this method can achieve very high theoretical efficiency with the actuator injecting a small amount of energy to account for impact losses.

Instead of utilizing the mechanical spring and damper, if virtual impedance is realized by electromagnetic torque control at the actuators, energy is recovered by electric regeneration, as demonstrated in electric cars. In this case, the parameters of virtual impedance (e.g. stiffness and damping coefficient) can be programmed in arbitrary form and adjusted instantly in a wide range starting from nearly zero impedance. Unlike mechanical damping that would dissipate all energy, the virtual damping impedance does not represent the energy dissipative element; it partially returns energy back to the source.

Efficient energy regeneration requires enhanced energy flow back into the battery, which also requires low impedance power transmission along the energy flow path from the foot to the battery. A low impedance power transmission path will also benefit power generation efficiency.

C. Principle 3:Low Impedance Mechanical Transmission

Employing gears significantly reduces the torque demands on the motors while increasing torque density. However, the addition of gearing adds reflected inertia and reflected damping of the actuator to the output shaft, and the values are multiplied by the square of the gear ratio. The increased mechanical impedance prevents the achievement of highly dynamic pro-prioceptive force control [16], and increases friction losses, which compromise the efficiency of energy regeneration during negative work.

However, it is difficult to generalize the optimization of the gear ratio for maximum energy efficiency. Employment of gear transmission increases gear friction, actuator mass, and leg impedance, but also reduces E_j by increasing the overall torque density. Such a design trade-off in a machine that has a constant angular speed can be easily characterized, but in legged locomotion, the characterization is much more involved, because legged locomotion requires highly dynamic interactions with the ground, and the transmission impedance will play a significant role in the overall dynamics of the robot. For example, increasing the gear ratio will reduce the joule heating but it will cause higher leg impedance and increase the impact loss. More importantly, it may limit the control of the robot dynamics. Moreover, such intricacy in this trade-off is highly variable depending on torque-speed trajectories of each joint, which are also a function of the speed of running, gait type, the scale of the robot and so on.

Gears introduce another subtlety of asymmetric friction loss, in which friction loss in the torque amplification direction is smaller than when energy flows back towards the motor [17]. This effect in spur gears has not been fully investigated; the full-gear model is part of the ongoing work of the MIT Cheetah project [18]. A full-gear interaction model is imperative for the simultaneous optimization of the actuator and gear selection to minimize losses.

For these reasons, in this article we propose to decouple the joule heating from the transmission design, and thus minimize the transmission impedance in order to maximize both the transmission efficiency and the impedance control capability. We will investigate the more accurate quantitative optimization method in the future.

D. Principle 4:Low Inertia Leg

As we often find slender legs on many biological runners, employing low leg inertia is critical for high-speed running. The low inertia leg allows higher bandwidth of the leg and, thus enables faster swing motion and higher stride frequency running. As a result, low leg inertia can reduce the torque requirements during the swing phase. Another benefit of light legs is to reduce impact loss at touch down at every step. A large portion of the kinetic energy of the leg should be dissipated not only in the cyclic motion in leg swing but also when the legs collide with the ground. We believe that these effects contribute how many animals evolved to have such slender legs.

The leg impact losses account for a significant amount of the energy loss in a running robot. Inelastic impact loss for simple linear motion is given in (1) where ΔP is the impulse from impact, v^+ and v^- are the velocities of before and after impact respectively and m is the impact mass. A more detailed model for jointed robots can be found in [19].

$$mv^+ = mv^- + \Delta P$$
$$E_i = -\Delta E = -\frac{m}{2}[(v^+)^2 - (v^-)^2] \tag{1}$$

Equation (1) suggests two ways to mitigate impact losses: by minimizing the change in velocity at impact, and by reducing the impact mass. As the impact velocity is related to the robot's relative velocity, one approach to reducing impact losses is to control the retraction speed of the leg before impact on the ground [20]. Another way to decrease impact losses is to reduce the impact mass. A lower distal mass is desirable for minimizing impact and also reduces the energy required to cycle the legs.

These four principles were implemented in the design of the MIT Cheetah, as shown in Fig. 2. Detailed implementation is explained in the next Section.

III. IMPLEMENTATION OF DESIGN PRINCIPLES ON THE MIT CHEETAH ROBOT

A. Large Gap Radius Motor

While maintaining the mass of the motor constant, the torque density of the motor can be improved by increasing the gap radius: the radius of the gap between the motor stator windings and the permanent magnets on the rotor. Seok et
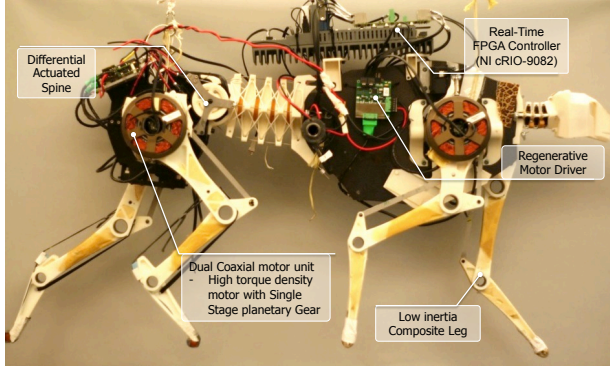
Fig. 4: Side view of the MIT Cheetah Robot showing design principles as implemented in hardware.

al. [16] has shown that the gap radius is a principal measure of motor performance. The analysis is performed with the assumptions that the rotor and stator maintain constant radial thickness, the mass stay constant and that the average shear stress applied to the rotor stays constant (see Fig.5). The torque density scales by approximately $\tau/m \propto r_{gap}$, the torque per inertia scales by $\tau/J \propto r_{gap}^{-2}$, and the torque squared per electric power, also known as motor constant square, a measure of torque production efficiency, scales by $\tau^2/I^2R = K_M^2 \propto r_{gap}^3$. Therefore, in a design space where the motor mass and the continuous torque requirement are held constant while the gap radius is free to vary and the massless and frictionless gear train are added to meet the torque requirement, the output torque and total reflected inertia are independent of the gap radius and corresponding gear ratio. This result indicates that if the analysis includes gear inertia, gear friction, as the gap radius of the motor increases, the results will favor the motor with the larger gap radius because it will have a smaller gear ratio and fewer gear-train stages; this results in less friction loss, higher torque density, and higher bandwidth. Therefore, in this particular design space, there is no trade-off.

Using this insight, a custom three-phase synchronous motor is designed as hown in Fig. 20, which is optimized for peak torque density for high speed running [21] (gap radius: 48.5 mm, torque constant: 0.4 Nm/A, weight: 1kg, phase resistance: 0.26 Ω, peak torque: 30Nm). The continuous torque density of this motor is also about 1.5 times compared with the
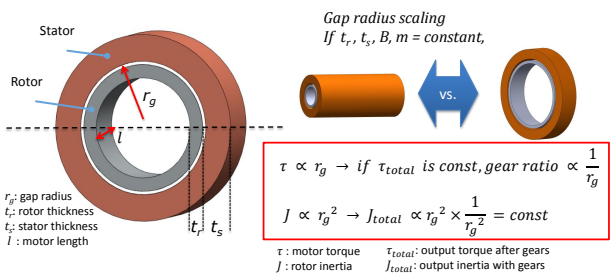
commercial motor currently used in the MIT Cheetah (Emoteq HT-5001, gap radius: 38.5 mm, torque constant of 0.27 Nm/A, weight: 1.3 kg, phase resistance: 0.354 Ω, peak torque: 10Nm).

B. Motor Drive Electronics Design for Regeneration

In order to realize efficient bidirectional energy flow, we employ proprioceptive force-control actuators [16]. This approach allows programmable leg impedances and high bandwidth control of large forces in a simple structure without series compliance and force sensors. The variable stiffness of the leg was tested and showed that it can realize radial stiffnesses of up to 10 kN/m, and damping ratios of up to 100 Ns/m.

In order to allow for energy regeneration in electromagnetic conversion, the architecture of the motor driver on the MIT Cheetah is designed to act like a bidirectional buck-boost converter [22]. Specifically, the motor driver on the MIT Cheetah robot is a custom switching converter built from three half bridges, capable of driving a three phase motor at 60A from a 100V supply. When energizing the motor, the motor driver bucks down the battery supply voltage to the desired phase voltages of the brushless motor [23]. In regenerative braking mode, the driver acts as a boost converter to step up the motor phase voltages to more than 100 VDC and recharge the batteries. This process is represented in Fig. 6.

The motor driver used on the MIT Cheetah robot commands voltages to each motor lead using pulse with modulation (PWM). Here, we designate the duty cycle as D and the applied motor voltage as Dv_{batt}. In the backward power flow direction, the motor driver is a boost converter and the stepped-up voltage is $\frac{1}{D}v_{bemf}$ where v_{bemf} is the back-EMF of the motor. If $\frac{1}{D}v_{bemf} > v_{batt}$ then the energy from braking the motor recharges the batteries.

To verify the effective regeneration during negative work, a simple experiment was performed. The MIT Cheetah robot was commanded to hold a fixed position with one leg held by a virtual spring with proportional gain of 5 kN/m and virtual damping of 100 Ns/m. Then, to simulate the impact that occurs during running, the robot was lifted and dropped onto the one leg being commanded to hold a constant position. The data from the experiment, shown in Fig. 7, confirm that the batteries were indeed recharged. The voltage of the battery line shown in Fig. 7(a) experienced a voltage spike from the

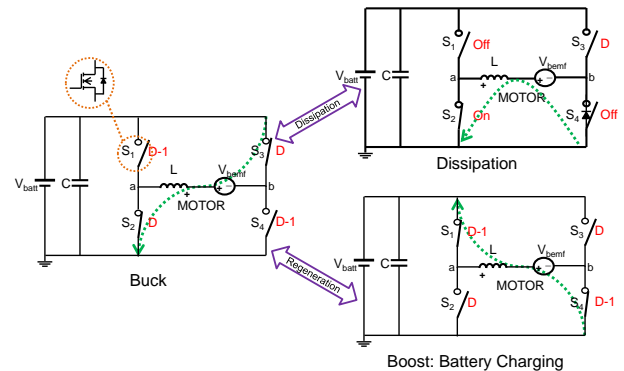Fig. 5: Gap radius scaling of electromagnetic motor with a constant mass.

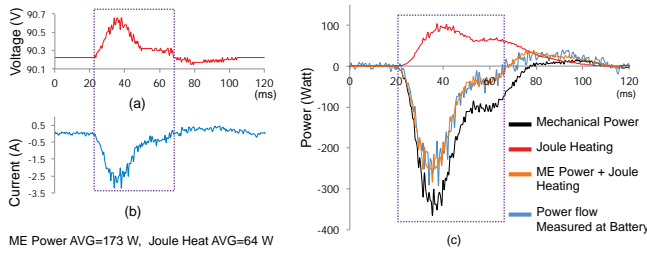Fig. 6: Energy flow in a Bidirectional Buck Boost Converter.

Fig. 7: (a) Voltage of the battery supply line during the regeneration experiment. (b) Current flowing out of the batteries during the regeneration experiment. (c) The mechanical power, Joule heating dissipation and battery power measured during experiment. Note that 63% of the negative mechanical work done by the motors is recovered by the batteries in the experiment.
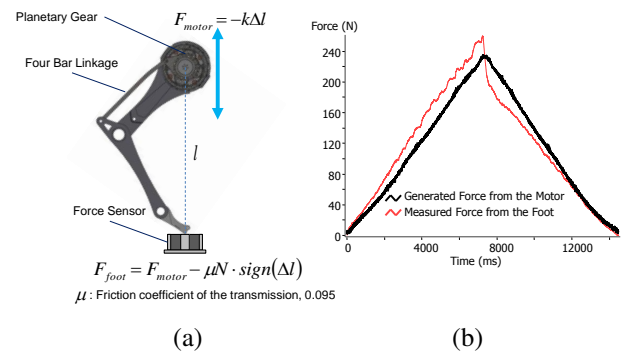

Fig. 8: (a) The experimental setup used for determining loss in the mechanical transmission. The force at the foot is calculated using the torques applied by the motors and compared against a force sensor under the foot. (b) Experimental data showing the difference between the expected force on the foot as generated from the motors, and the actual force measured.

boosted motor voltage and Fig. 7(b) clearly shows current flow back into the battery. Fig. 7(c) accounts for the mechanical work done by the motor, the amount of the Joule heating in the motor windings and the power consumption at the batteries. Sixty-three percent of the negative mechanical work done by the motors was recovered by the batteries in the experiment. The charging efficiency of lithium polymer batteries can be over 95% [24], showing that most of the regenerated energy goes into recharging the batteries. However, in most steady state running cases, the regenerated energy from one motor is fed to other motors. This is shown in the data in Fig. 15; there is a brief moment when the total power from the battery is zero, but not negative.

C. Low Gear Ratio Transmission

To minimize the losses associated with cascading gear loss, the number of gear stages is restricted to only one stage in each motor. A single gear stage in a commercial gearbox can lose approximately 10% of the input power [25]. This value is dependent on the gear quality and detailed parameters of gear, such as module, pressure angle, and so on. In general, a higher gear ratio will have a higher friction loss, but increasing the number of gear train stages significantly increases friction, overall inertia of the gears, backlash, and complexity of the structure. For example, it is more desirable to have a higher gear ratio in one stage than to split it into two stages. Thus, the MIT Cheetah robot uses a custom designed single stage of planetary gearing with a gear ratio of 5.8:1 on each motor, the largest ratio that can be obtained at a single stage in the given space. The relatively low ratio reduces the contribution of reflected actuator dynamics on the impedance of the transmission output. However, this gear ratio is not optimized due to the lack of a detailed loss model.

The friction of the mechanical transmission needs to be measured to determine its effect on proprioceptive control [16]. A diagram of the experimental setup is shown in Fig. 8(a). The leg was subjected to a compression and decompression cycle applied externally by a linear material testing device. The motors were commanded to act as a virtual spring to resist the compressive force of the machine. We measured the

expected output force from the motor current and compared it to the force at the foot as measured by a commercial force sensor. The two forces are shown in Fig. 8(b) and the transmission loss is modeled as a force-dependent coulomb loss acting against the direction of travel. The resulting friction coefficient is 0.095, equivalent to 9.5% power loss.

D. Biotensegrity Leg

As a part of the effort to minimize leg inertia, we implemented a bio-inspired leg design approach in the MIT Cheetah, namely, a tendon-bone co-location architecture [26]. We hypothesized that the bones of the animals legs carry mostly compressive loads while the muscles, tendons and ligaments carry the tensile loads [27]. This distribution makes effective use of the relative advantages of each biological material to achieve a lightweight yet strong structure. To achieve this same tendon-bone co-location architecture, a tendon was integrated into the design of the MIT Cheetah leg, linking the foot to the knee. Experiments show that this architecture reduces the stress experienced by the bone during stride by up to 59%. A composite bone-like structure of the robot leg was fabricated drawing inspirations from biological structures. A rigid and light polyurethane foam-core for the leg was covered in a high stiffness polyurethane resin to form a composite with high strength but low inertia. Further details on the tendon-bone co-location design architecture and experiments performed on the robot leg can be found in [26].

E. Dual Coaxial Motor Design

Observations of biological running animals such as horses show that most of the musculature in the legs is concentrated proximal to the shoulder of the animal. Based on the inspiration from this observation, the architecture of the leg of the MIT Cheetah is specifically designed to minimize inertia. Two motors are placed co-axially in the shoulder: one motor actuates the shoulder joint while the other actuates the knee through the use of a four-bar steel linkage. The center of mass
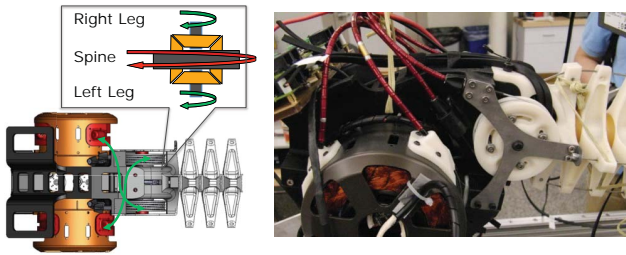
Fig. 9: Spine Differential Cabling. As the MIT Cheetah runs, the steel cables couple the motions of the rear legs to the motions of the spine in the sagittal plane. The green color arrows indicate how the cabling couples each leg to the differential input shafts, which then drive the center drum to actuate the spine.
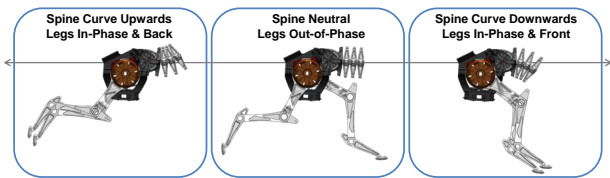

Fig. 10: Differential Spine Actuation. During high speed running, the spine can be actuated by choosing to actuate the rear legs either in-phase or out-of-phase. When the legs are in-phase and backward, the differential coupling would cause the spine to arch upwards, increasing the stride length of the MIT Cheetah. When the legs are in-phase and forward, the differential would make the spine curve downwards, tucking the rear legs further forward. Otherwise, when the legs are out-of-phase, the spine remains neutral.

is 45 mm from the center of rotation [16]. This architecture is in contrast to the traditional serial link architecture shown in many humanoid robot arms, where the actuators are located at every joint, increasing the inertia of the distal links which is not conducive to high speed running. Such architecture also benefit in proprioceptive force control by minimizing inertial forces of the legs under high acceleration. The architecture of Phantom was designed under using a similar principle [28].

F. Differential Actuated Spine

A switchable spine mechanism was implemented in the design of the MIT Cheetah to explore the effect of the spine in the dynamics of running. We specifically designed the spine actuation mechanism to select among rigid, passive, and actuated modes. The spine is made up of rings of polyurethane rubber sandwiched by spine vertebrae segments. In the actuated or passive mode, the polyurethane rubber disks can store elastic energy and return it during galloping. Through the innovative use of a differential, the spine is actuated without the necessity of an extra actuator, which would require a large torque and hence add a large mass. Instead, the motions of the two rear legs are coupled to the motion of the spine through the differential as seen in Fig. 9. This mechanism significantly reduces the total mass of the robot, which enhances the energy

efficiency and allows for fair comparison among running performances with rigid, passive, and actuated spines.

With the differential actuated spine, the robot can actively arch its spine up and down in the sagittal plane and cover more ground in one stride that it would otherwise with a rigid back. When the front legs hit the ground, the spine is also able to absorb some of the impact and store it as a bending force in the urethane rubber rings that bring the front legs forward. This is demonstrated in Fig. 10. Through this novel use of the spine, it is hoped that highly efficient, high speed locomotion is achieved.

IV. EXPERIMENT

This section shows the experimental results of a test of the trotting gait of the MIT Cheetah. The current running speed is 6m/s (13.5mph) and mechanically constrained to stay in the sagittal plane. The robot is powered by a battery and the dummy weight of the battery is loaded on the robot simulating the battery mass. The next subsection briefly explains the running algorithm, the subsection IV-B explains the experimental setup, and the subsection IV-C discusses the results of the running experiments.

A. Control Algorithm

A new control algorithm for high-speed quadrupedal locomotion has been developed for the MIT Cheetah. This algorithm consists of a pattern modulator, a gait-trajectory generator and an impedance controller. The foot trajectory for the experiment is as shown in Fig.11.
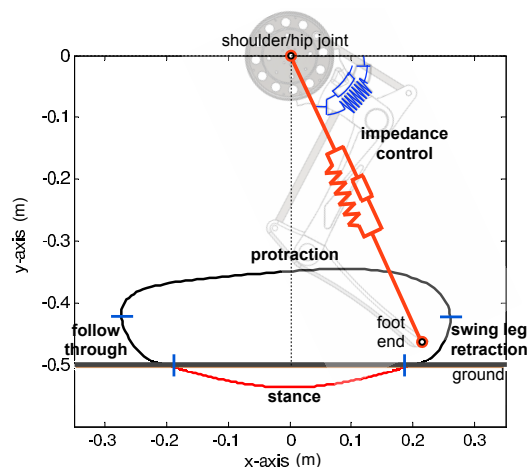

Fig. 11: Desired swing phase(black solid line) and stance phase(red solid line) trajectory for the front leg, as well as the desired ground position(straight black solid line at -0.5 m). The point $(0, 0)$ is the location of shoulder/hip of the robot.

The trajectory consists of two parts: swing phase and stance phase. We fixed the desired swing time as 250 ms, and decreased the desired stance time from 850 ms to 60 ms for increased speed. Each foot was controlled by the impedance controller, and the virtual impedance gains commanded by the controller are listed in Table.I. The pattern modulator
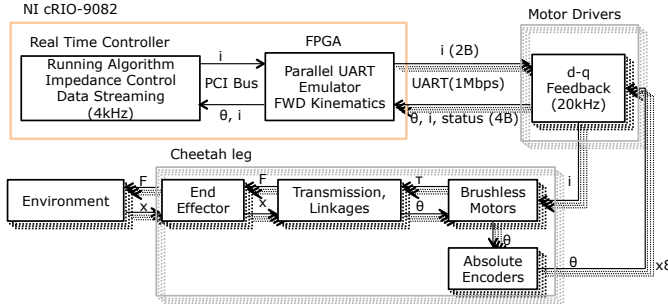
Fig. 12: Control System Diagram for the MIT Cheetah Robot. The main controller (NI cRIO-9082) has the Real-Time multicore controller and the FPGA and controls 8 BLDC motor drivers in parallel.
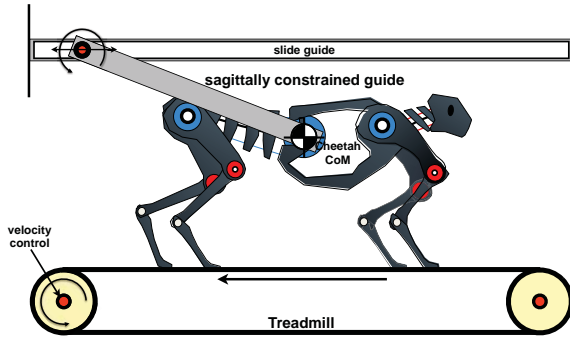

Fig. 13: Experimental setup of MIT Cheetah on treadmill. Motion is constrained to the sagittal plane.

can describe various animal gait patterns by synchronizing individual legs to a specific pattern with a target speed; for the test in this paper, a trot gait was used. The chosen gait pattern was triggered when the left front foot of the robot touched the ground and generated one stride. This process was repeated while the robot was running, and it successfully modulated the gait pattern over different speeds. The gait generator matches the pattern signals given from the pattern modulator to the predefined foot-end trajectory for each leg. And by the impedance controller, tracking control for the swing phase and the contact compliance control for the stance phase are executed. This algorithm allows for stable trot running up to the limit of the treadmill speed (6m/s).

	Description	Value
$K_{p,r}$	Virtual radial stiffness	5,000 N/m
$K_{d,r}$	Virtual radial damping	100 Ns/m
$K_{p,\theta}$	Virtual angular stiffness	100 Nm/rad
$K_{d,\theta}$	Virtual angular damping	4 Nms/rad

TABLE I: Impedance gain values for the experiment

B. Experimental Setup

An experimental setup was constructed to facilitate the testing of the MIT Cheetah running. The MIT Cheetah runs on the commercial fitness treadmill (SOLE TT8) that has been modified to be 3.5m long to accommodate the length of the robot. The treadmill has a 3.5 horse power DC

motor(TURDAN DC.PM 90V-25A), and is controlled by a NI sbRIO-9642 with a motor driver (Apex Microtechnology MSA260KC). The treadmill speed is measured by a rotary encoder (CUI Inc AMT 102-V) directly attached to the DC motor's axis. The treadmill speed is manually adjusted by changing the PWM frequency, and the treadmill is powered by lithium polymer batteries connected in series, providing 148V DC. With this input voltage, the maximum speed of the treadmill is 6 m/s, which limits the test speed of the running robot. A linear guiderail system is mounted above the treadmill. A pair of rail sliders is attached to the robot via metal bars and a rod that goes through its center of mass (CoM). This configuration ensures that the motions of the MIT Cheetah are constrained within the sagittal plane without any roll and yaw, but the robot is free to move in both vertical and fore-aft translation and to rotate along the pitch axis. For safety, the batteries were not located on the robot, but a 3 kg dummy mass was added to the cheetah body to simulate the battery weight. A figure representing the experimental setup can be seen in Fig. 13.

The control system is comprised of four layers of controllers: the motor drivers, the parallel UART emulators, the Real-Time multicore controller, and the monitoring PC. Each motor driver (MCU: Microchip dsPIC30F6010) handles the current control of one BLDC motor at 20 kHz. The 12 parallel UART emulators are programmed in the FPGA (Spartan-6 LX150) for communication with eight custom brushless DC motor drivers and four Dynamixel EX-106+ smart motors. The Real-Time multicore controller (i7 dual-core 1.33 GHz) has two CPUs with three roles. CPU 0 which manages parallel UART communication in the FPGA layer runs a high priority loop at 4 kHz. It also logs all the Data to an embedded Compact Flash Card with about 1 MB/s writing speed in a normal priority loop. CPU 1 computes all the running algorithms and impedance control in a high priority loop runs at4 kHz. The PC is used for monitoring and changing parameters of the system wirelessly through the 802.11 protocol. The NI cRIO-9082 houses both the FPGA layer and the Real-Time multi controller, and all the software is programmed by NI LabVIEW. Control hardware is shown in Fig. 4, and the system diagram is shown in Fig. 12.

C. Experimental Results

We measured the the voltage and the current data of each motor and the treadmill speed. The estimated speed from the robot and the treadmill speed has a 0.15 m/s bounded error, so the estimated data is used for the following analysis. High-speed video is captured at 500 fps by a high-speed camera (Mikrotron MC1363) with the NI PCIe-1429 frame grabber. Captured running images can be seen in Fig. 14.

The change in power consumption for two cycles at 6 m/s is shown in Fig. 15. Mechanical power, Joule heating and total power were calculated using the Equations 2. The previous research [13] and Fig. 7.(c) proved that power consumption measured at battery matches up with the sum of Mechanical Power+Joule Heating, so the power consumption at the battery is not plotted in the Fig.15. The power consumption by the motor drivers is included in Joule heating.

Fig. 14: High-speed video captured at 500 fps depicting 150ms of the MIT Cheetah running at 6 m/s.

TABLE II: MIT Cheetah power consumption values during 6 m/s running

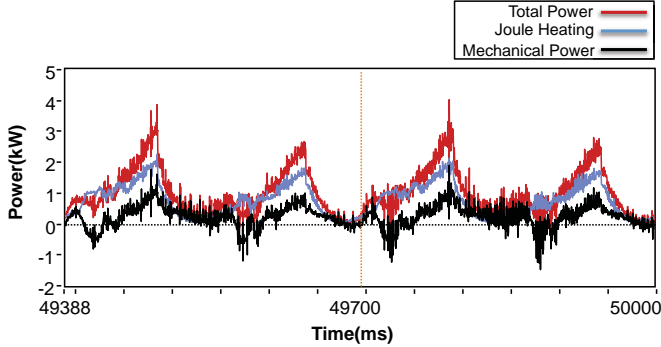| Total Power	Joule Heating	Mechanical Power		COT	with **3 Kg** Battery (465 Whrs)	
					Running Time	Distance
973 W	739 W (76%)	**234 W (24%)**		0.5	0.48 Hrs	10.3 km
		Positive	Negative			
		292 W	-58 W			

Fig. 15: Power Consumption during 6 m/s trotting of the MIT Cheetah. The blue line is the power used in Joule heating. The black line is mechanical power. The red line represents the total power consumption, which is the sum of Joule heating and mechanical power.

It can be seen that the mechanical power(black line) showed negative values which were regenerated during locomotion. This regenerated power was supposed to charge the battery or be consumed in the other legs. The total power briefly reached zero but did not go negative, which means that the generated energy when a pair of legs do negative work was fed to the other pair of legs to do positive work. In most gaits, we expect that most regenerated energy goes to other joint actuators and that little energy recharges the batteries. However, in several exceptional cases, such as during the ground phase in a pronk gait or landing from jumping, we expect that a significant amount of energy will charge the batteries.

$$
\begin{aligned}
\text{Mechanical Power} &= \sum\nolimits_{8 \text{ motors}} \tau \times \omega \\
&= \sum\nolimits_{8 \text{ motors}} K_t \times I_{motor} \times \omega \\
\text{Joule Heating} &= \sum\nolimits_{8 \text{ motors}} I_{motor}^2 R \\
\text{Total Power} &= \text{Mechanical Power} + \text{Joule Heating}
\end{aligned}
\tag{2}
$$

One of the most remarkable results in this experimentation is that Joule heating, which results in 76% of total power, is by far the predominant mode of power consumption. Table II shows several attributes of the average power consumption at 6 m/s. Of the 973 W consumed, 739 W is lost in Joule heating, while 234 W is consumed by the net mechanical work, which is dissipated through gear friction, joint friction, and interaction loss. From this data we can predict that the MIT

Cheetah robot can run 10.3 km with 3 kg (465 Whrs) LiPo Battery. Although the large contribution of the Joule heating loss can be mitigated by increasing the gear ratio, such an approach may cause other problems, such as added complexity in mechanisms, added mass, increased reflected inertia, higher impact loss, and poorer impedance control.

The MIT Cheetah weighs 33 kg and the TCoT is 0.5, which is similar to that of other biological runners of similar mass. Fig. 1 shows the TCoT of animals in nature as well as man-made vehicles. The TCoT of representative robots are overlaid [3] to compare the metabolic energy consumption of animals with the overall power consumption of mobile robots. For animal data, the three classes of locomotion (runners, fliers, and swimmers) occupy distinct regions of the plot of TCoT versus body mass. As seen in the graph, the MIT Cheetah robot is right below the runners' line which means its energy efficiency is similar to that of a biological runner of similar mass.

We observed an interesting trend in Fig. 16.(a) that shows the change in TCoT as the MIT Cheetah accelerates from 1 m/s to 6 m/s in a trot. So far, no biological runners of a similar scale have been observed to trot up to this speed, possibly because the trot is energetically much more expensive than other gaits such as canter or gallop. The Froude numbers[3] between 2.0 to 3.0 is the region where the second transition happens from trot to canter or gallop [29]. The energetic cost data in horses shows that horses have a preferred speed for trot and if their trot speed deviates from that speed, the TCoT increases and they switch to another gait if it is more efficient. Interestingly, the TCoT of the MIT Cheetah decreases continuously up to 6 m/s. The TCoT may increase after a certain higher speed but this phenomenon is not yet examined in this test. For this particular controller, the robot's 'preferred speed' of trot is higher than 6 m/s. Such high-speed trotting requires a high stride frequency and high-speed leg motion, which are usually not desirable in animals. The major reason that explains this result might be the characteristic difference between electromagnetic motors and biological muscle. For example, muscles have a distinct force-displacement and a force-velocity constraints described by Hill's model [30], but torque of electric motors is independent from its position

---

[3]The Froude number is the ratio of the centripetal force around the center of motion, the foot, and the weight of the animal/robot. It can be calculated by v^2/gl, where v is the velocity, g is the acceleration due to gravitiy, and l is the characteristic length of the leg.

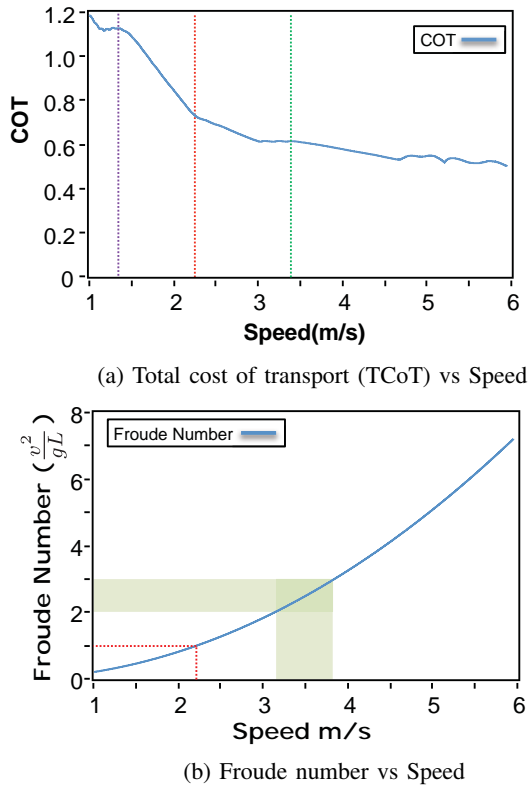(a) Total cost of transport (TCoT) vs Speed

(b) Froude number vs Speed

Fig. 16: The plot shows TCoT and Froude number with respect to running speed from 1 m/s to 6 m/s. (a) The red line indicates the start of running (2.3m/s). The green line shows when the swing leg retraction speed reaches 3.4 m/s. (b) The red line represents a Froude number of 1.0, where animals switch from walk to run. For the MIT Cheetah robot, the Froude number of 1 corresponds to 2.3 m/s, the speed at which the robot switches from walk to run. The green area is the region of Froude numbers between 2.0 and 3.0 where quadrupeds change the gait from trot to gallop
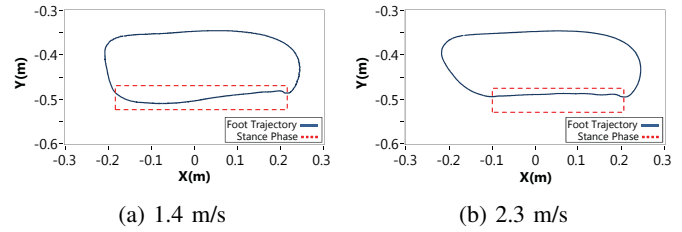

Fig. 17: The plots show measured foot trajectory with the same coordination in the Fig. 11. The blue line represents the measured foot trajectory, and the red dotted box represents the stance phase. (a) The plot is one cycle trajectory at 1.4 m/s where the duty factor is 0.5. (b) The plot is at 2.3 m/s where the shoulder height from the ground starts reaching its lowest point near mid-stance.
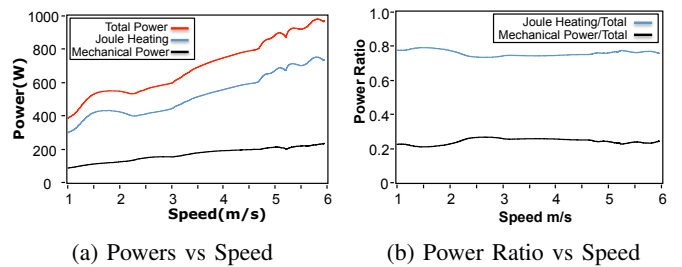

Fig. 18: The plot shows Joule heating and mechanical power, and the ratios between them with respect to running speed from 1m/s to 6m/s. (a) The red line represents the total power consumption from the battery, which is the sum of Joule heating and mechanical power. The blue line is the power used in Joule heating. The black line is the mechanical power. (b) The blue line is the ratio of Joule heating to the total power, and the black line is the ratio of mechanical power to the total power. The ratios are not changed significantly with respect to speeds.

and velocity, assuming that we have an electric source whose voltage is high enough.

During the period when the duty factor (the fraction of a stride during which a given foot is on the ground) goes under 0.5 (from 1 m/s to 1.4 m/s), the TCoT drops and becomes stationary. From 1.4 m/s to 2.3 m/s, the TCoT drops rapidly. At 2.3 m/s, the MIT Cheetah starts running[4] as shown in the Fig. 17 and this corresponds to a less steep decrease in TCoT. At 3.4 m/s the swing leg retraction speed is increased to match the ground speed, and the TCoT remains stationary at the region around the speed of 3.4 m/s. The minimum TCoT reached is 0.5025 at 5.95 m/s.

At 2.3 m/s, which corresponds to a Froude number of 1, the gait typically changes to running, as shown in Fig. 16.(b). When the Froude number is around 1.0, the centrifugal force equals to gravitational force, and most animals switch from walking gaits to running gaits [29], and the same transition is

shown in the Cheetah robot.

Although the MIT Cheetah's running gait is not optimized for efficiency, it shows an exceptional mechanical cost of transport (MCoT). MCoT is calculated based on mechanical work instead of total power consumption; note that the mechanical work only counts total positive work and doesn't substrate out the negative work [11]. Researchers who have an interest in optimizing the gait pattern and trajectory for efficiency tend to use MCoT for showing the performance of their robots. The MIT Cheetah has MCoT of 0.15 at 6 m/s which is around 10 times better than the Honda ASIMO (MCoT 1.6) [33], and its performance is similar to that of the energy-optimized robot MABEL (MCoT 0.14) which has an external power source and a real-time controller [33] whereas the MIT Cheetah has everything inside. Moreover, it exceeds the efficiency of animals of similar weight, such as dogs and goats (MCoT 0.2 at 2.85 m/s trot) [34].

However, as discussed in the introduction, it is critical for robot designers to consider the TCoT, including not only mechanical power but also other dissipative energy losses such as Joule heating. Fig. 18 shows the change in power

---

[4]Here, we follow McMahon and McGeer's definition of running[31], [32]. In running, midstance is the instant of minimum height, in other words, the center of mass reaches its lowest point near midstance.
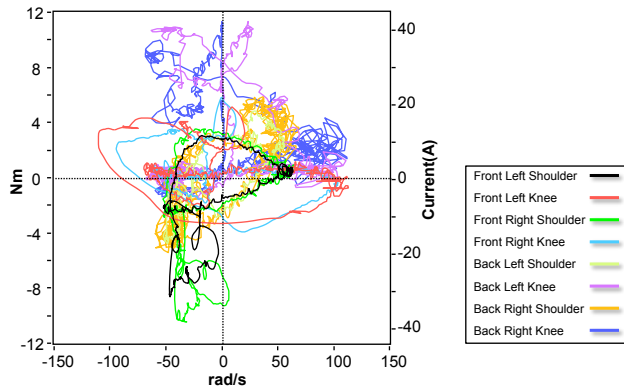
Fig. 19: Plot of Angular Velocity vs Motor Torque at 6 m/s. The black line represents the front left shoulder (FLS) motor, and the dark blue line represents the back right knee (BRK) motor.

Fig. 20: Newly developed MIT motor and MIT Cheetah v.2

consumption as the MIT Cheetah accelerates from 1 m/s to 6 m/s in a trot gait. It can be seen that Joule heating accounts for roughly 75% of the energy consumption from the battery over the whole range of speed. The ratio of mechanical power to the total power consumption is only about 25%, which is independent from energy loss from the actuators and highly depends on the control algorithms. These data suggest that for any legged robots, the design of the motor is critical to increasing efficiency. Specifically, use of high torque-density motors, as described in Section II-A, is directly related to this goal of minimizing heat dissipation.

Energy regeneration is essential for increasing the efficiency of the MIT Cheetah, since there are non-negligible negative powers regenerated by the motors. Fig. 19 shows the change in angular velocity versus motor torque in the motors of the MIT Cheetah at 6 m/s. The angular velocity multiplied by torque becomes mechanical power as in the Equations 2. The activities in the top-right and bottom-left quadrants represent exertion of positive power, and the activities in top-left and bottom-right quadrants represent exertion of negative power. Specifically, the top-left quadrant is where the foot hits the ground and negative work happens. The amount of power in this region is regenerated from the motor drivers and circulates to alternating motors to do positive work. Apart from the discussion of energy regeneration, this plot will be very useful in the design of motors for a running legged robot.

V. CONCLUSIONS AND FUTURE WORK

Based on the energy flow of a locomotive system, four major design principles were highlighted and successfully implemented to the MIT Cheetah. The principles include high torque-density motors, an energy regenerative electronic system, low loss transmission, and low leg inertia. The MIT Cheetah achieved a cost of transport of 0.5 that rivals running animals and is significantly lower than other running robots. From the experimental results, specifically analysis of energy loss in the components of the system, we learned that Joule heating is the major power loss during locomotion. In order to reduce the Joule heating from electric motor, we have
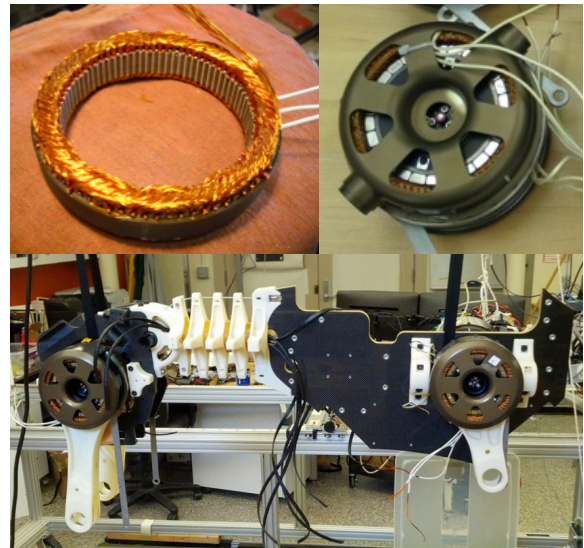
developed a new custom-designed 3-phase motor, shown in Fig. 20 focused on reducing heat loss and maximizing torque density. The preliminary experiment data shows that it has 3 times the saturation (peak) torque, 1.5 times the torque constant and 0.73 times the phase resistance of the current motor. When these new motors are implemented on the MIT Cheetah robot, it is expected that the TCoT will be reduced to 0.25, which is superior to efficiency of biological runners and similar to that of fliers in nature.

ACKNOWLEDGMENT

REFERENCES

[1] P. Bhounsule, J. Cortell, and A. Ruina, "Design and control of ranger: An energy-efficient, dynamic walking robot," in *CLAWAR 2012 - Proceedings of the Fifteenth International Conference on Climbing and Walking Robots and the Support Technologies for Mobile Machines*, July 2012, pp. 441–448.

[2] V. A. Tucker, "The energetic cost of moving about: Walking and running are extremely inefficient forms of locomotion. much greater efficiency is achieved by birds, fishand bicyclists," *American Scientist*, vol. 63, no. 4, pp. pp. 413–419, 1975.

[3] A. Ruina. (2012, September) Cornell ranger 2011, 4-legged bipedal robot. [Online]. Available: http://ruina.tam.cornell.edu/research/topics/locomotion_and_robotics/ranger/Ranger2011/

[4] O. Auro and P. Komi, "The mechanical efficiency of pure positive and pure negative work with special reference to the work intensity," *International Journal of Sports Medicine*, vol. 7, pp. 44–49, 1986.

[5] R. Tedrake, T. Zhang, M. Fong, and H. Seung, "Actuating a simple 3d passive dynamic walker," in *Robotics and Automation, 2004. Proceedings. ICRA '04. 2004 IEEE International Conference on*, vol. 5, april-1 may 2004, pp. 4656 – 4661 Vol.5.

[6] J. Hurst, J. Chestnutt, and A. Rizzi, "The actuator with mechanically adjustable series compliance," *Robotics, IEEE Transactions on*, vol. 26, no. 4, pp. 597–606, 2010.

[7] M. Hutter, C. Gehring, M. Bloesch, M. Hoepflinger, C. D. Remy, and R. Siegwart, "Starleth: A compliant quadrupedal robot for fast, efficient, and versatile locomotion," in *Int. Conf. on Climbing and Walking Robots (CLAWAR)*, 2012.

[8] S. Kim, J. Clark, and M. Cutkosky, "isprawl: Design and tuning for high-speed autonomous open-loop running," *The International Journal of Robotics Research*, vol. 25, no. 9, pp. 903–912, 2006.

[9] S. Wolf and G. Hirzinger, "A new variable stiffness design: Matching requirements of the next robot generation," in *Robotics and Automation, 2008. ICRA 2008. IEEE International Conference on*, may 2008, pp. 1741 –1746.

[10] S. K. G. Folkertsma and S. Stramigioli, "Parallel stiffness in a bounding quadruped with flexible spine," in *IEEE/RSJ International Conference on Intelligent Robots and Systems*, October 2012.

[11] P. Bhounsule, J. Cortell, B. Hendriksen, J. Karssen, C. Paul, and A. Ruina, "A robot that walked 65 km on a single charge: energy-effective and reliable locomotion using trajectory optimization and stabilization from reflexes," *Submitted to The International Journal of Robotics Research*, 2012.

[12] D. Renjewski, A. Spröwitz, and J. Hurst, "Atrias-a human size compliant bipedal robot walks efficiently."

[13] S. Seok, A. Wang, Chuah, M. Y. (Michael), D. Otten, J. Lang, and S. Kim, "Design principles for highly efficient quadrupeds and implementation on the mit cheetah robot," in *2013 IEEE International Conference on Robotics and Automation*, 2013.

[14] A. Ruina, J. Bertram, and M. Srinivasan, "A collisional model of the energetic cost of support work qualitatively explains leg sequencing in walking and galloping, pseudo-elastic leg behavior in running and the walk-to-run transition," *Journal of Theoretical Biology*, vol. 237, no. 2, pp. 170 – 192, 2005.

[15] M. Yoong, Y. Gan, G. Gan, C. Leong, Z. Phuan, B. Cheah, and K. Chew, "Studies of regenerative braking in electric vehicle," in *Sustainable Utilization and Development in Engineering and Technology, 2010 IEEE Conference on*, nov. 2010, pp. 40 –45.

[16] S. Seok, A. Wang, D. Otten, and S. Kim, "Actuator design for high force proprioceptive control in fast legged locomotion," in *IEEE/RSJ International Conference on Intelligent Robots and Systems*, October 2012.

[17] M. Dohring, E. Lee, and W. Newman, "A load-dependent transmission friction model: theory and experiments," in *Robotics and Automation, 1993. Proceedings., 1993 IEEE International Conference on*, may 1993, pp. 430 –436 vol.3.

[18] A. Wang, "Directional Impedance of Geared Transmissions," Master's thesis, Massachusetts Institute of Technology, 2012.

[19] I. Walker, "The use of kinematic redundancy in reducing impact and contact effects in manipulation," in *Robotics and Automation, 1990. Proceedings., 1990 IEEE International Conference on*, may 1990, pp. 434 –439 vol.1.

[20] M. Haberland, J. Karssen, S. Kim, and M. Wisse, "The effect of swing leg retraction on running energy efficiency," in *Intelligent Robots and Systems (IROS), 2011 IEEE/RSJ International Conference on*, sept. 2011, pp. 3957 –3962.

[21] N. Farve, "Design of a low-mass high-torque brushless motor for application in quadruped robotics," Master's thesis, Massachusetts Institute of Technology, 2012.

[22] F. Caricchi, F. Crescimbini, F. Capponi, and L. Solero, "Study of bi-directional buck-boost converter topologies for application in electrical vehicle motor drives," in *Applied Power Electronics Conference and Exposition, 1998. APEC '98. Conference Proceedings 1998., Thirteenth Annual*, vol. 1, feb 1998, pp. 287 –293 vol.1.

[23] D. Torres and P. Heath, "Regenerative braking of bldc motors," Microchip Technology Inc., Tech. Rep.

[24] Z. Salameh and B. Kim, "Advanced lithium polymer batteries," in *Power & Energy Society General Meeting, 2009. PES'09. IEEE*. IEEE, 2009, pp. 1–5.

[25] F. Faulhaber, "A second look at gearbox efficiencies," *Machine Design*, pp. 82–84, June 2002.

[26] A. Ananthanarayanan, M. Azadi, and S. Kim, "Towards a bio-inspired leg design for high-speed running," *Bioinspiration and Biomimetics*, vol. 7, no. 4, p. 046005, 2012.

[27] K. Rudman, R. Aspden, and J. Meakin, "Compression or tension? the stress distribution in the proximal femur," *BioMedical Engineering OnLine*, vol. 5, no. 1, p. 12, 2006.

[28] T. H. Massie and J. K. Salisbury, "The phantom haptic interface: A device for probing virtual objects," in *Proceedings of the ASME winter annual meeting, symposium on haptic interfaces for virtual environment and teleoperator systems*, vol. 55, no. 1. IOS Press, 1994, pp. 295–300.

[29] R. M. Alexander, "The gaits of bipedal and quadrupedal animals," *The International Journal of Robotics Research*, vol. 3, no. 2, pp. 49–59, 1984.

[30] A. Hill, "The heat of shortening and the dynamic constants of muscle," *Proceedings of the Royal Society of London. Series B, Biological Sciences*, vol. 126, no. 843, pp. 136–195, 1938.

[31] T. A. McMahon, G. Valiant, and E. C. Frederick, "Groucho running," *Journal of Applied Physiology*, vol. 62, no. 6, pp. 2326–2337, 1987.

[32] T. McGeer, "Passive bipedal running," *Proceedings of the Royal Society of London. B. Biological Sciences*, vol. 240, no. 1297, pp. 107–134, 1990.

[33] K. Sreenath, H.-W. Park, I. Poulakakis, and J. W. Grizzle, "A compliant hybrid zero dynamics controller for stable, efficient and fast bipedal walking on mabel," *The International Journal of Robotics Research*, vol. 30, no. 9, pp. 1170–1193, 2011.

[34] D. V. Lee and A. A. Biewener, "Bigdog-inspired studies in the locomotion of goats and dogs," *Integrative and comparative biology*, vol. 51, no. 1, pp. 190–202, 2011.